ORIGINAL ARTICLE

Biomechanical study of different plate configurations for distal humerus osteosynthesis

M. Bogataj · F. Kosel · R. Norris ·
M. Krkovic · M. Brojan

Abstract Fractures of the distal humerus are most commonly fixed by open reduction and internal fixation, using plates and screws, either in a locking or in a non-locking construct. Three different plating systems are commonly used in practice. The most important differences between them are in plate orientation, which affects both the rigidity of the osteosynthesis and invasiveness of the surgical procedure. Unfortunately, there is no common agreement between surgeons about which plate configuration brings the best clinical outcome. In this study, we investigate the theoretical rigidity of plate osteosyntheses considering two types of AO/ASIF configurations (90° angle between plates), Mayo clinic (Acumed) configuration (180° between plates) and dorsal fixation of both plates. We also compared the results for cases with and without contact between the bone fragments. In the case of no bone contact, the Mayo clinic plate configuration is found to be the most rigid, followed by both AO/ASIF plate configurations, and the least rigid system is the Korosec plate configuration. On the other hand, no significant differences between all types of fixation configurations are found in cases with contact in-between the bone fragments. Our findings show that this contact is very important and can compensate for the lack of load carrying capacity of the implants. This could therefore incite other implant fixation solutions, leading to less invasive surgical procedures and consequently improved clinical outcome.

1 Introduction

Distal humerus fractures are relatively rare injuries representing 2–6 % of all fractures and 30 % of fractures in the elbow region of the human body [13]. It is known that these types of fractures are challenging to stabilize in orthopedic trauma surgery [14]. Current standard treatment for displaced intraarticular fractures of the distal humerus is open reduction and exercise-stable internal fixation, in the vast majority of cases with plates and screws. It is important that the stabilization of bone fragments is rigid enough to allow early postoperative motion. Longer durations of immobilization usually result in unsatisfactory elbow function [14]. The Association for Osteosynthesis/Association for the Study of Internal Fixation (AO/ASIF, AO Foundation, 2012) recommends an orthogonal plate configuration (two combinations of approximately 90° angle between plates are available), whereas Mayo clinic (Acumed, 2012; [23]) recommends a close to 180° configuration of plates for distal humeral fracture fixation. Access to the distal humerus demands a certain level of exposure as soft tissues are dissected. The more the plates are pushed toward

M. Bogataj · F. Kosel · M. Brojan (✉)
Laboratory for Nonlinear Mechanics, Faculty of Mechanical
Engineering, University of Ljubljana, Askerceva 6,
1000 Ljubljana, Slovenia
e-mail: miha.brojan@fs.uni-lj.si

R. Norris
University Hospitals Coventry and Warwickshire, Clifford Bridge
Road, Coventry CV2 2DX, UK

M. Krkovic
Addenbrookes Hospital, Cambridge University Hospitals NHS
Foundation Trust, Cambridge Biomedical Campus, Hills Road,
Cambridge CB2 0QQ, UK

the anterior (volar) part of the distal humerus (closer to 180° between plates) the greater the dissection of soft tissues that is required, causing higher operative trauma with early and late postoperative consequences (scarring, limited range of movement, tardy ulnar nerve palsy, etc.). B. F. Korosec from University Clinical Center, Ljubljana, developed a less invasive surgical procedure to treat distal humerus fractures placing both plates on the dorsal side of the distal humerus, which considerably reduces the possibility of postoperative complications [15].

There is no common agreement between surgeons about which plate configuration brings the best clinical outcome. Different (in vitro) experimental studies characterizing the mechanical response of the osteosyntheses using aforementioned plate configurations are available in the literature. For example, Schwartz et al. [25] made a comparison between the two most commonly used plating systems (Mayo clinic and AO/ASIF) fixed on composite bones. They found no statistical differences in stiffness, in any load direction. Korner et al. [14] compared the osteosynthesis of the AO/ASIF and dorsal plate configurations using cadaver specimens. The systems were subjected to three individual loading conditions: pure bending, pure torsion and pure axial compression. Cyclic bending and load to failure were also tested. The AO/ASIF configuration was found to be more rigid when subjected to pure bending and pure torsion. When axial compression was applied, they found no statistical difference in stiffness. Cyclic loading did not reduce the rigidity of the system. Similarly, Penzkofer et al. [24] compared the rigidity of the Mayo clinic system and both combinations of AO/ASIF plate configurations, using composite bones. They found that the most rigid system was the Mayo clinic plate configuration, when applying the load on the distal end of the humerus in a perpendicular direction to its length. The same conclusion followed when the system was subjected to cyclic loading. When applying a load in an almost axial direction, the most rigid system was the AO/ASIF plate configuration with plates fixed on the medial and dorsolateral side of the humerus. Furthermore, Zalavras et al. [31] made an experiment using cadaver specimens with the humerus, ulna and radius to test the rigidity of Mayo clinic and AO/ASIF type of fixation. They found that Mayo clinic plate configuration was the most rigid when cyclic torsion was applied. This plate configuration also withstood higher failure loads when subjected to loading in a flexion and extension plane. In contrast to these experimental investigations, clinical research studies of the problem are rare. We found only one such paper, by Shin et al. [26] who made a clinical comparison between the Mayo clinic and AO/ASIF plate configuration. They observed no significant differences between both configurations in terms of clinical outcomes and complication rates.

Building on the commonalities of these studies which consider physical experiments with simplified loading and assuming only the cases with a gap at the fracture site, we set up a theoretical model including the effect of contact between the bone fragments (no gap in-between the bone fragments) and loading conditions similar to those that occur during exercise (applying them quasi-statically). The model combines analytical (principle of virtual work) and numerical calculations (finite element analysis, FEA). We compare all four types of plate fixation mentioned above, the Mayo clinic 180° plate configuration, the two systems of orthogonal fixation of AO/ASIF-type plates and the Korosec dorsal configuration and analyze the differences in rigidity of each osteosyntheses construct emanating from the plate orientation, and the effects of the invasiveness of the surgical procedure.

According to the best of the authors' knowledge, this study is the first attempt in the literature using a numerical approach (although a wealth of other finite-element-based analyses of different osteosynthesis problems can be found, e.g., see [1, 5, 10, 17, 27]) to show how the contact between the bone fragments affects the rigidity of the distal humerus fracture osteosynthesis, altogether as a function of the plate orientation. We find that in cases with a gap between the fracture fragments, the most rigid configuration is the Mayo clinic plate configuration, followed by both AO/ASIF plate configurations, and the least rigid system is the Korosec plate configuration. In cases with no gap in-between the bone fragments, we found no significant differences in rigidity between all four types of plate configuration. Our findings show that the contact between the bone fragments is very important and can compensate for the lack of load carrying capacity of the implants. This could incite other implant fixation solutions, leading to less invasive surgical procedures and consequently improved clinical outcome.

2 Methods

2.1 Geometry and material properties of bone and implant models

A finite element model with a simulated fracture at the distal end of the humerus (see Fig. 1) was set up in Abaqus CAE 6.10-1 (Dassault Systèmes, France). Main fracture profile was modeled after the 13-C2 fracture type of Müller AO classification of long bone fractures (articular component is simple, and the metaphyseal component is multifragmentary). Smaller fragments were neglected in our study to simplify the calculation and avoid a high number of contacts and long computing times. The bone model as shown in Fig. 1a) is based on a point cloud, which
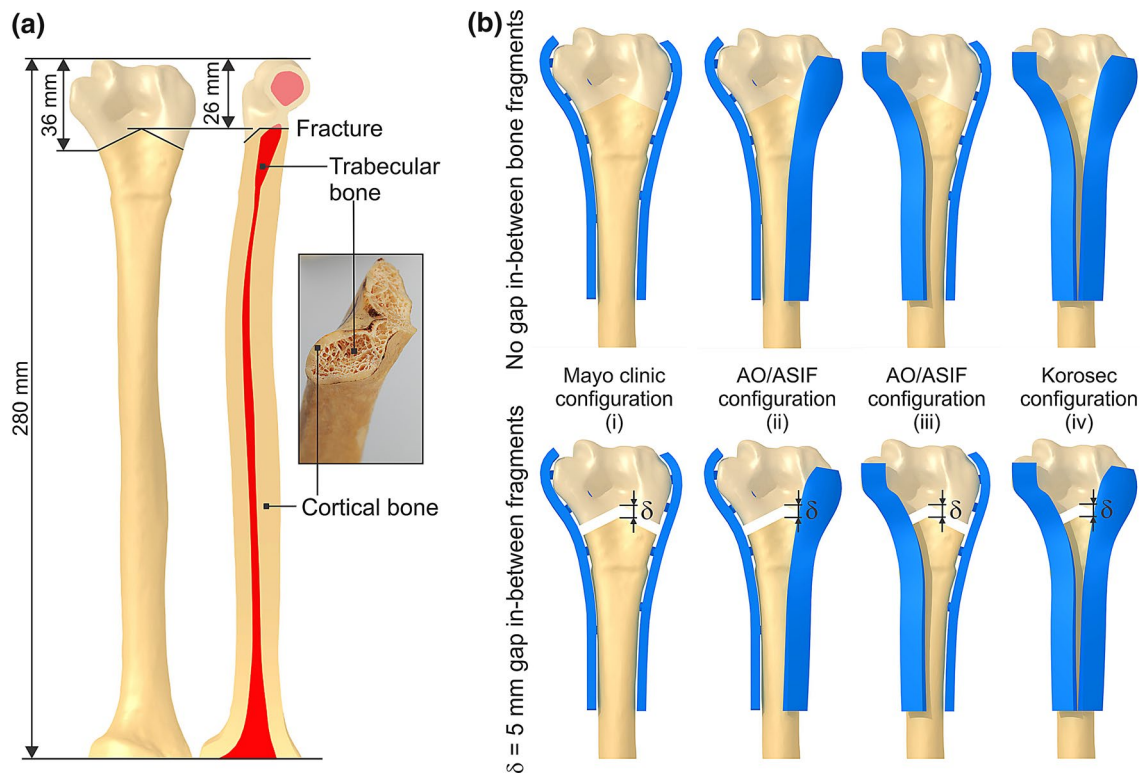
Fig. 1 Osteosynthesis construct geometry: **a** bone geometry—cortical and trabecular bone regions are modeled separately in Catia V5 and coupled together in Abaqus CAE. **b** Different plate configurations in a case with no gap between bone fragments (*first row*) and in a case with 5-mm gap between bone fragments (*second row*)

represents the humeral surface generated from CT images (Siemens Sensation 16, resolution: 512 × 512, pixel size: 0.488 mm). The upper extremity of one 45-year-old male was measured in University Medical Centre Ljubljana to generate bone surface mesh in *.wrl* format. The format was changed to *.stl* in MeshLab V1.3.0 (Visual Computing Laboratory, Italy) and imported into Catia V5 (Dassault Systèmes, France). The cortical and trabecular bone regions were modeled as homogenized solids. The cortical bone thickness was measured in Mimics 10.01 (Materialise, Belgium) from CT scans and divided into three parts along the length, in which the thickness was well approximated by a constant along the epiphysis (2.5 mm), the diaphysis (6.5 mm) and a linear function in-between (see supplementary material, diagram in Fig. S1). This enabled us to model the cortical bone simply, with an offset from the outer surface of the point cloud in each of the three parts. Note that the error of this particular approximation is within the limits of measuring scatter of real bone geometries from different patients.

Four different virtual models of bone plates were designed in Catia: lateral plate, medial plate, dorsolateral plate and dorsomedial plate, as illustrated in Fig. 1b). All plates were modeled to have the same material properties,

the same rectangular 4 × 10 mm cross-section at the fracture site and the same configuration of screws (there was one difference though, in the most proximal screw, between medial and lateral plates where crossing of screws in the bone had to be avoided, see supplementary material, Fig. S2, for a detailed view). Such "normalization" of plates eliminated the differences between designs from different manufacturers and enabled us to investigate the plate configuration effect on the system response alone. It is important to note that screws and bone plates were modeled as one solid piece (cylinders with 4 mm in diameter), which simulates locking plates and simplifies the osteosynthesis model. Stiffness of osteosynthesis systems using locking plates versus conventional reconstruction plates has previously been compared by Korner et al. in [14], who found that stiffness depends more on the plate configuration than on the type of plates. This implies that the results of our study apply for both, locking and non-locking plate types.

Osteosynthesis plates were attached to the bone with screws, tied (tie constraint in Abaqus CAE) to pre-created holes in the humerus. According to Wieding et al. [30], this type of screw simulation gives up to a 95 % correlation between experimental and numerical results and gives relatively accurate displacement results on the global level, but

less accurate stress–strain prediction around the holes, as discussed in the paper [18]. Local stresses around the screw holes are important for screw loosening prediction (simulated in Ref. [9]), which may also affect clinical outcome.

For each type of plate configuration, we created models of osteosynthesis with a gap and no gap at the fracture site, as shown in Fig. 1b). We considered:

1. Mayo clinic plate configuration that represents 180° angle in-between lateral and medial plates,
2. AO/ASIF configuration that represents a dorsolateral plate and a medial plate (90° angle in-between plates),
3. AO/ASIF configuration that represents a dorsomedial plate and a lateral plate (90° angle in-between plates),
4. and the Korosec plate configuration that represents dorsolateral and dorsomedial plates.

A 5-mm gap size was modeled on all four configurations (1)–(4) to simulate a comminuted fracture with no contact between bone fragments, which is similar to the experimental studies listed above. In these studies, small fragments do not transfer any load between the diaphysis and the rest of the bone. For example, Korener et al. [14] considered a 5-mm gap, Penzkofer et al. [24] considered a 6-mm gap and Zalavras et al. [31] considered a 10-mm gap to simulate metaphyseal comminution. To study how the contact between the bone fragments affects the rigidity of the distal humerus fracture osteosynthesis (as a function of the plate orientation), we additionally considered the cases without a gap in-between the fragments in all four configurations (1)–(4).

Bone plates and screws were assumed to be made from austenitic stainless steel AISI 316L/DIN 1.4404/X2 CrNiMo17-12-2 ($E \cong 210$ GPa, $\nu = 0.3$, cf. eFunda, 2012). Mechanical properties of the cortical bone were approximated to be homogeneous, isotropic and non-porous, although the real tissue possesses far more complex biomechanical properties. The Young's modulus $E_c = 20$ GPa and the Poisson ratio $\nu_c = 0.3$ were used for the cortical bone, based on Vandenbulcke [28, 29]. The cortical bone density $\rho_c = 2,000$ kg/m^3 was considered [28]. Mechanical properties of the trabecular bone are more complex and needed to be simplified, since the tissue is highly porous, and the density changes with the position in the bone [7]. The non-homogeneous distribution of trabecular bone density ρ_{tr} was measured on CT images in Mimics 10.01, based on the Hounsfield number, which was calibrated on the cortical bone density. The Young's modulus of trabecular bone E_{tr} is closely related to ρ_{tr}, [12]. The relationship between E_{tr} and ρ_{tr} is given by the equation $E_{tr} = 2,915\rho_{tr}^3$, where ρ_{tr} is density given in g/cm^3 and E_{tr} in MPa [12]. It was observed that E_{tr} varied in our study from 0^+ to approximately 1,000 MPa (see Fig. S3 in Supplementary material), which showed a good correlation with the experimental data published by

Dunham et al. [6], where the E_{tr} in the distal humerus was measured to vary from 2.9 to 1,041.7 MPa. For the sake of simplicity, the trabecular bone was also modeled as a homogenized solid and further approximated to be constant $E_{tr} = 500$ MPa. Sensitivity analysis reveals (see Table S1 and Fig. S4 in the Supplementary material) that trabecular bone properties have limited effect on the results of our study due to large difference in elastic moduli of cortical and trabecular bone parts (more that 20:1). Variation of E_{tr} between 0^+ and 1,000 MPa (i.e., the min. and max. values that we calculated from the densities, as explained above) and subjecting the bone to one of the loading cases during flexion showed that the difference in maximum recorded bone displacement using $E_{tr} = 0$ and $E_{tr} = 1,000$ MPa was well within 0.5 %. A complete removal of the trabecular bone would simplify the model even more (resulting in decreased computing time), but would also result in almost no contact surfaces between the bone and screws, and in-between bone fragments.

2.2 Loading conditions

Exact loading conditions of bones in the upper extremity are difficult to determine due to the complex array of muscles responsible for movement, complex geometry and material properties, which vary in the longitudinal direction as well as over the cross-section and depending on the current upper extremity position. Different musculoskeletal models of the upper extremity were discussed in previous papers [2]. Nikooyan et al. [22] described the development of one of them, the deft shoulder and elbow model (DSEM), used it to predict the relative muscle forces and compared the results with their normalized EMG signals. For the purposes of our study, loads acting on the humerus were determined using the method of virtual work and calculated for the particular model of the human upper extremity as shown in Fig. 2a). Bones were modeled as beams, loaded with moments, as well as axial and shear forces. The humerus thus represents a cantilever beam, fixed at the proximal end by muscles which are otherwise responsible for humeral movements (*m. deltoideus*, *m. pectoralis major*, *m. latissimus dorsi*, *m. teres major*, *m. subscapularis*, *m. supraspinatus*, *m. teres minor* and *m. infraspinatus* [20]). In the elbow, one degree of freedom was assumed—a rotation that enables flexion and extension. The difference in loading of the humerus during pronation and supination of the forearm was neglected (only supination was considered), even though there is slightly different muscle activity [11]. The mass of the upper arm was taken into account in the model as a continuously distributed load over the humerus, and the mass of the forearm was considered as a continuously distributed load over the radius and ulna. The 20 N point load was assumed to act in the wrist, and also its mass was added to the load.
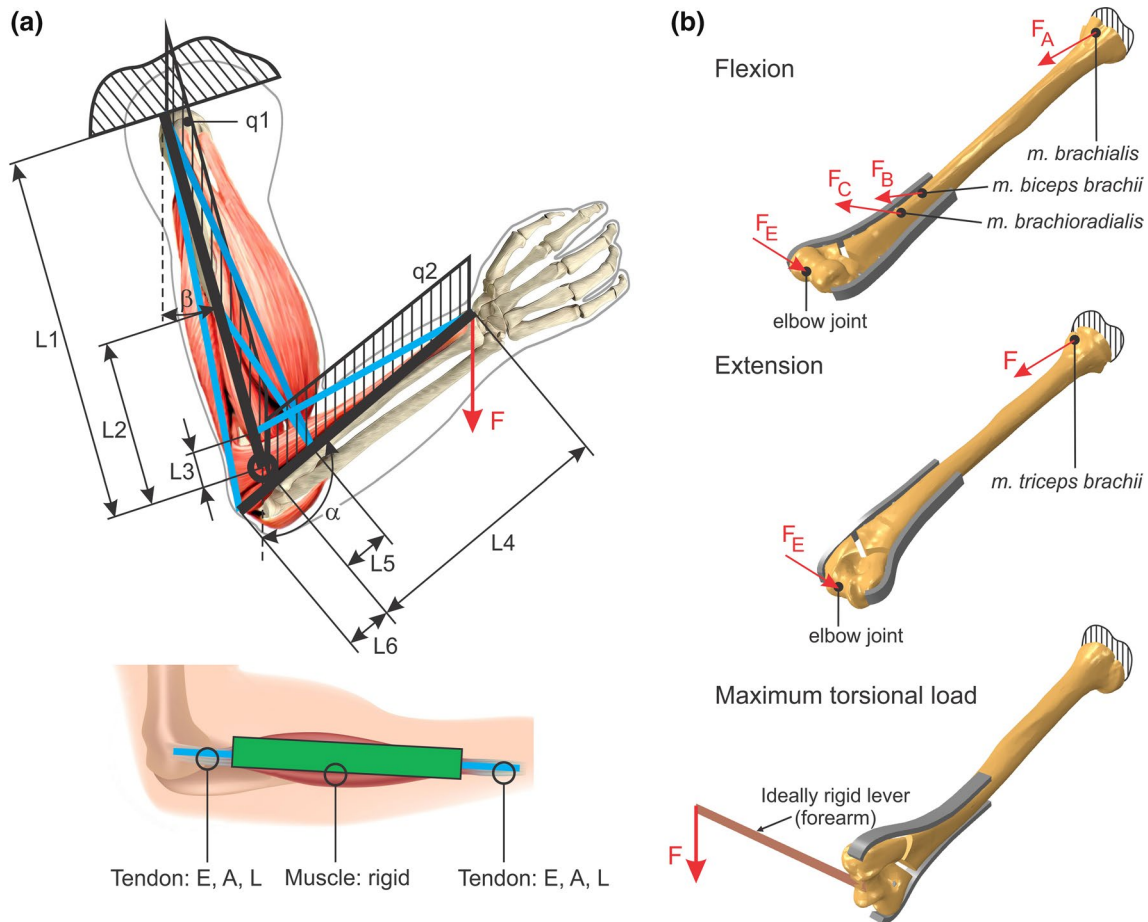
Fig. 2 Modeling: **a** detailed model of human upper extremity as a standard engineering construction (*above*) and a simplified model of a muscle–tendon unit (*below*). **b** Loading conditions of the osteo-synthesis construct and boundary conditions: Forces in the muscles and in the elbow joint were calculated via virtual work method and applied as point forces in FE model

We investigated the three different upper extremity movements most commonly used during rehabilitation. The first one was flexion, a movement that describes a bending that decreases the angle between the forearm and the upper arm. The second movement was extension, which is the opposite of flexion and increases the angle between both parts of the upper limb. The third movement simulates lifting and carrying a glass of water to the mouth generating a large torsional load. During flexion, the construction is two times statically undetermined. To solve this subproblem of calculating muscle forces, we used the method of virtual work, employing geometry of the system and material (geometrical and material specifications were obtained from different sources, as cited in Table 1). At this stage of the model, we assumed a uniform circular cross-section of the bones and the mechanical properties of the cortical bone only. Muscles, on the other hand, are not passive structures like bones [21] and have very complex material properties. We modeled them as rigid elements with adjustable lengths depending on the current upper

extremity position. Tendons that connect muscles to bones and carry only tension forces were approximated as cables (their geometric and material properties were found in the literature, see Table 1). Different muscles are active during different movements. During flexion, muscles on the anterior side of the humerus are active: *m. biceps brachii*, *m. brachialis* and *m. brachioradialis* [8]. Other muscles are also active, but their role is mainly to assist and can be ignored for the purposes of our study. During extension, only one muscle was taken into account (*m. triceps brachii*), which makes the construction statically determined. There are some other muscles on the dorsal side that are active [8], but their influence can also be neglected. Movement simulating maximum torsion load comprised only one position of upper extremity—the force acting perpendicular to the forearm, see Fig. 2b). For this purpose, an ideally rigid 250-mm-long lever, representing the forearm, was modeled and attached to the elbow joint. Torsional moment of 8.75 Nm was applied as a 35 N load acted at the end of the lever.

Table 1 Geometrical and material properties

Symbol	Value	Meaning	Literature
L1	310 mm	Humerus length	[7]
L2	103.3 mm	*m. brachialis* insertion into the humerus	[7]
L3	77.5 mm	*m. brachioradialis* insertion into the humerus	[7]
L4	250 mm	Radius/ulna length	PRL-S[a]
L5	30 mm	*m. biceps brachii* and *m. brachialis* insertion into the radius/ulna	[8]
L6	15 mm	*m. triceps brachii* insertion into the ulna	[8]
m1	2.23 kg	Male upper arm average mass	[12]
m2	1.39 kg	Male forearm average mass	[12]
m3	0.52 kg	Male wrist average mass	[12]
q1	0.0706 N/mm	Continuously distributed load over humerus	Calculated
q2	0.0545 N/mm	Continuously distributed load over radius/ulna	Calculated
l1	50 mm	Tendon length in *m. biceps brachii* muscle–tendon unit	Estimated from anatomical drawings [20]
l2	20 mm	Tendon length in *m. brachialis* muscle–tendon unit	Estimated from anatomical drawings [20]
l3	100 mm	Tendon length in *m. brachioradialis* muscle–tendon unit	Estimated from anatomical drawings [20]
E_{tendon}	600 MPa	Tendon Young's modulus	[4, 19]
A_{tendon}	20 mm^2	Tendon cross-sectional area	[4, 19]
D1	23 mm	Middle humerus diameter	PRL-S[a]
D2	16 mm	Middle radius diameter	PRL-S[a]
D3	10 mm	Middle ulna diameter	PRL-S[a]
I1	13,737 mm^4	Moment of inertia of humerus cross-section	Calculated
I2	3,708 mm^4	Moment of inertia of radius/ulna cross-section	Calculated
ρ_c	2,000 kg/m^3	Cortical bone density	[28]
E_c	20 GPa	Cortical bone Young's modulus	[28, 29]
ν_c	0.34	Cortical bone Poisson's ratio	[28, 29]
ρ_{tr}	0–700 kg/m^3	Trabecular bone density	Measured
E_{tr}	0–1,000 MPa	Trabecular bone Young's modulus	Calculated
E	210 GPa	Stainless steel Young's modulus	(eFunda, 2012)
ν	0.3	Stainless steel Poisson's ratio	(eFunda, 2012)

[a] *PRL-S* Pacific Research Laboratories-Sawbones, 2012 (internet source)

Note that forces were calculated for different positions of the upper extremity, defined with different combinations of angles α and β for flexion and extension movements. Here, angle α describes elbow flexion/extension, and angle β describes glenohumeral flexion/extension. Eighteen different positions of the upper extremity were defined with different combinations of angles α and β, roughly divided into two groups: in the first group, $\beta = 0°$ was kept constant and angle α varied between 9° and 81° with 9° step size; in the second group, $\alpha = 90°$ was kept constant and angle β varied between 0° and 72° with 9° step size.

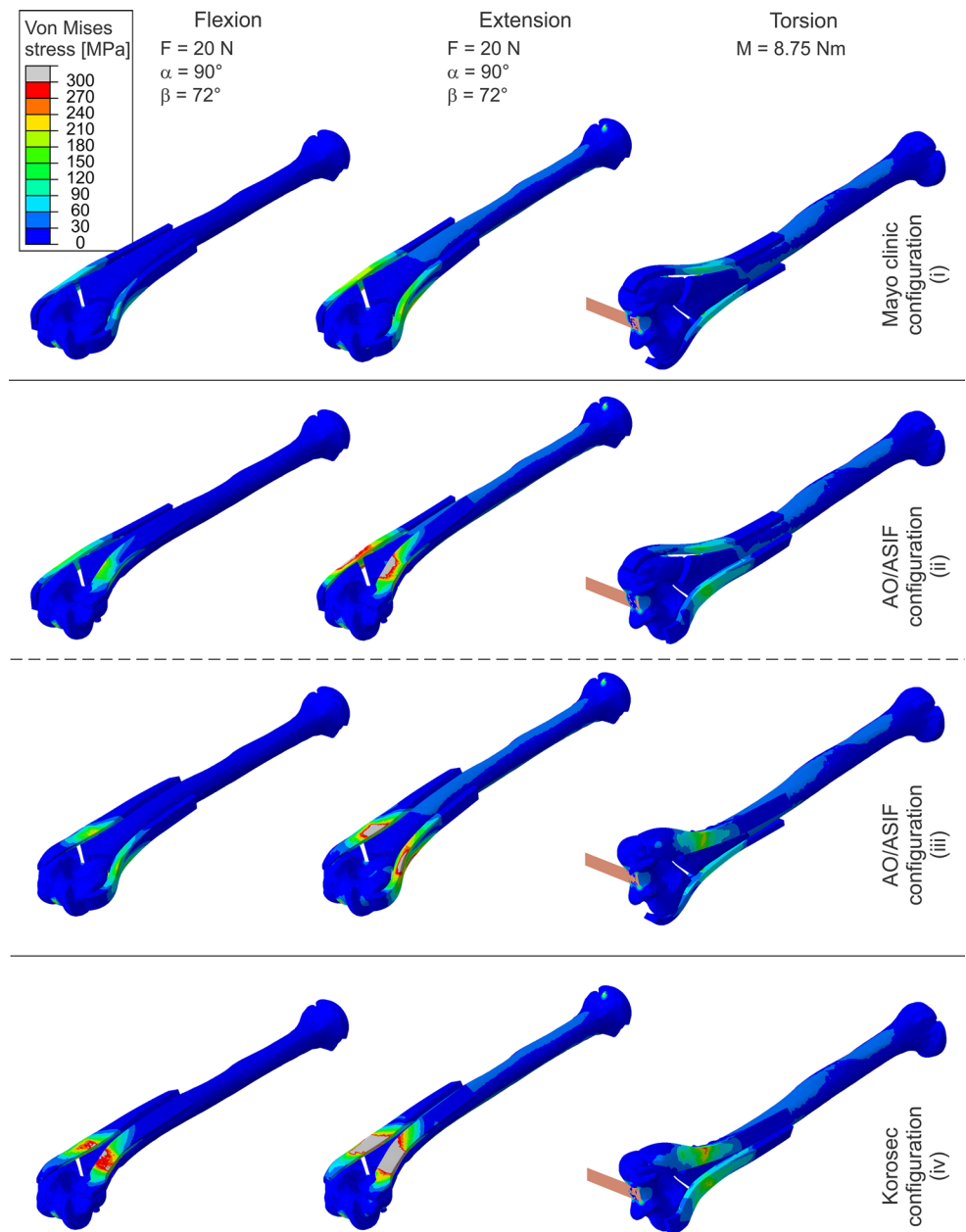### 2.3 Finite element model

Boundary conditions in the finite element model were the same as above; the humerus was fixed at the proximal end, as shown in Fig. 2. Forces calculated via virtual work method were applied as point forces at the positions as shown in Fig. 2b). Hard contact with no friction was defined on the fracture surfaces. Tetrahedral finite elements were used for all parts in osteosynthesis. Quadratic tetrahedral elements C3D10 are known to give better solutions when the number of elements is lower (cf. supplementary material, Fig. S6). Due to complex geometry and to simplify the meshing effort, we used linear tetrahedral elements C3D4 with finer meshes, instead. All models were meshed in the same way, having fine meshes on plates and regions around holes, and coarse meshes in the proximal humerus and trabecular bone. All models had approximately 500,000 elements depending on positions of holes and the presence of the gap.

2.4 Numerical experimental procedure

From the set of 18 calculations of loading conditions for flexion and extension movements, nine, more

Fig. 3 Stress distributions in different osteosynthesis systems with 5-mm gap. Figure shows distributions when the load is applied in different loading regimes


critical combinations (from the second group, where angle $\alpha = 90°$), were considered and used in the finite element model. Each of these combinations of forces (and a torsional moment of 8.75 Nm, for the case of maximum torsion load) was applied in the FE model at the position where muscles are attached to the humerus or at the elbow joint, as shown in Fig. 2b). The mechanical response of each system was then calculated with Abaqus. We recorded the change in the fracture gap size δ (depicted in Fig. 1) and maximal plate stress (cf. Fig. 3). Gap size δ was defined as the minimal Euclidean distance in 3D between the fracture surfaces. The difference between gap sizes of the reference/unloaded and loaded system was then calculated and served as a measure

of rigidity: larger the change in gap size, the lower rigidity the system exhibits (and vice versa). Stress was not calculated to predict mechanical failure, but to study how each structure carries the load and how that correlates to the gap size change and rigidity of the osteosynthesis construct.

3 Results

3.1 Inner forces in the humerus

Extension/flexion muscle forces and inner forces in the humerus were calculated for a 20 N point load in the
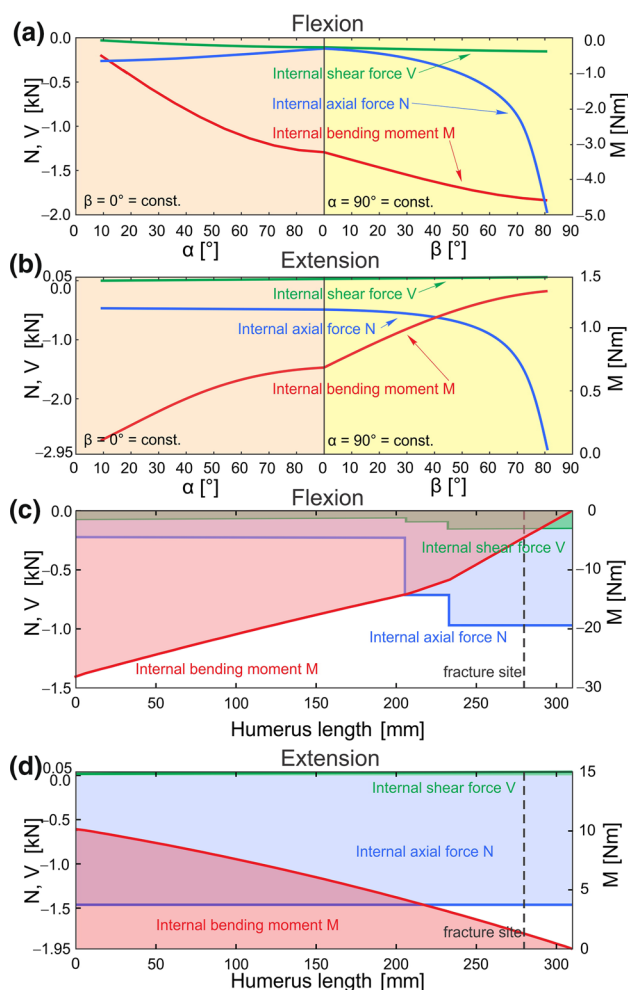
Fig. 4 Internal forces at the fracture site during: **a** flexion; **b** extension. Inner forces in humerus during **c** flexion (e.g., $\alpha = 90°$, $\beta = 72°$); **d** extension (e.g., $\alpha = 90°$, $\beta = 72°$)

wrist and for different upper extremity positions (defined by angles α and β). Changes in gap size and thus osteosynthesis stiffness depend mostly on internal forces at the fracture site. Figure 4a, b show diagrams of internal axial (N) and shear (T) forces and internal bending moment (M) at the fracture site as functions of angles α and β, respectively, for flexion and extension. We notice that the change of internal forces is more prominent when angle β is varied (rather than angle α). Maximal inner forces are found when α is 90° and β approaches 90°. As an example, Fig. 4c, d show diagrams of inner forces within the humerus at fixed $\alpha = 90°$ and $\beta = 72°$. In both cases, inner axial force is compressive and dominant over the inner shear force.

3.2 Finite element model with 5-mm gap

In the case of a gap where there is no contact between the bone fragments, this means that at the fracture site, the

plates are carrying all of the loads. (Note that, away from the fracture site, the bone is also carrying the load through the screws which fix the plates to the bone.) As expected, changes in gap size during flexion and extension are much higher on the anterior side than on the dorsal side, because there is always at least one plate on the dorsal side, except in the Mayo clinic plate configuration.

Figure 5a, b show changes in gap size during flexion and extension, respectively. From both diagrams, we can observe that the most rigid configuration (higher rigidity corresponds to smaller change in gap size and vice versa) is the Mayo clinic plate configuration, followed by both AO/ASIF plate configurations, and the least rigid system is the Korosec plate configuration. Figure 5c, d show maximal stresses within plates during flexion and extension, respectively. Stresses are increasing with increasing angle β. The stresses are higher in the least rigid system (Korosec) and lowest in the stiffest system (Mayo clinic), as expected from the results in Fig. 5a, b. When the bone is subjected to the torsion load, changes in gap size are significantly lower than during extension or flexion. In the case of 8.75 Nm torsion load, the maximum change is 0.02 mm.

3.3 Finite element model with no gap

In the case with no gap between the bone fragments, differences in gap size changes for the different plate configurations become negligible, as presented in Fig. 5a, b. During flexion, there are almost no differences in plate stress among the different plate configurations, as shown in Fig. 5c. During extension, the results in Fig. 5d show slight (practically negligible) differences. The largest stress appears in the Mayo clinic, and the lowest in Korosec plate configuration. Calculations of changes in gap size on the dorsal and anterior side during maximal torsion load (although not displayed in diagrams) show that the most rigid system is the Mayo clinic plate configuration and the least rigid is the Korosec plate configuration. Changes on dorsal side are smaller than 0.03 mm, and <0.07 mm on the anterior when subjected to an 8.75 Nm torsion moment.

4 Discussion

Displaced intraarticular fractures of the distal humerus are currently treated by open reduction and internal fixation, using plates fixed with screws in a locking and nonlocking configuration. Plates can be fixed on the humerus in different orientations. The most common type of fixation is configuration close to 180° between both plates (by Mayo clinic) and the one close to 90° between plates (by AO/ASIF). Another configuration, suggested by B. F. Korosec, is a fixation of both plates on the dorsal side [15,
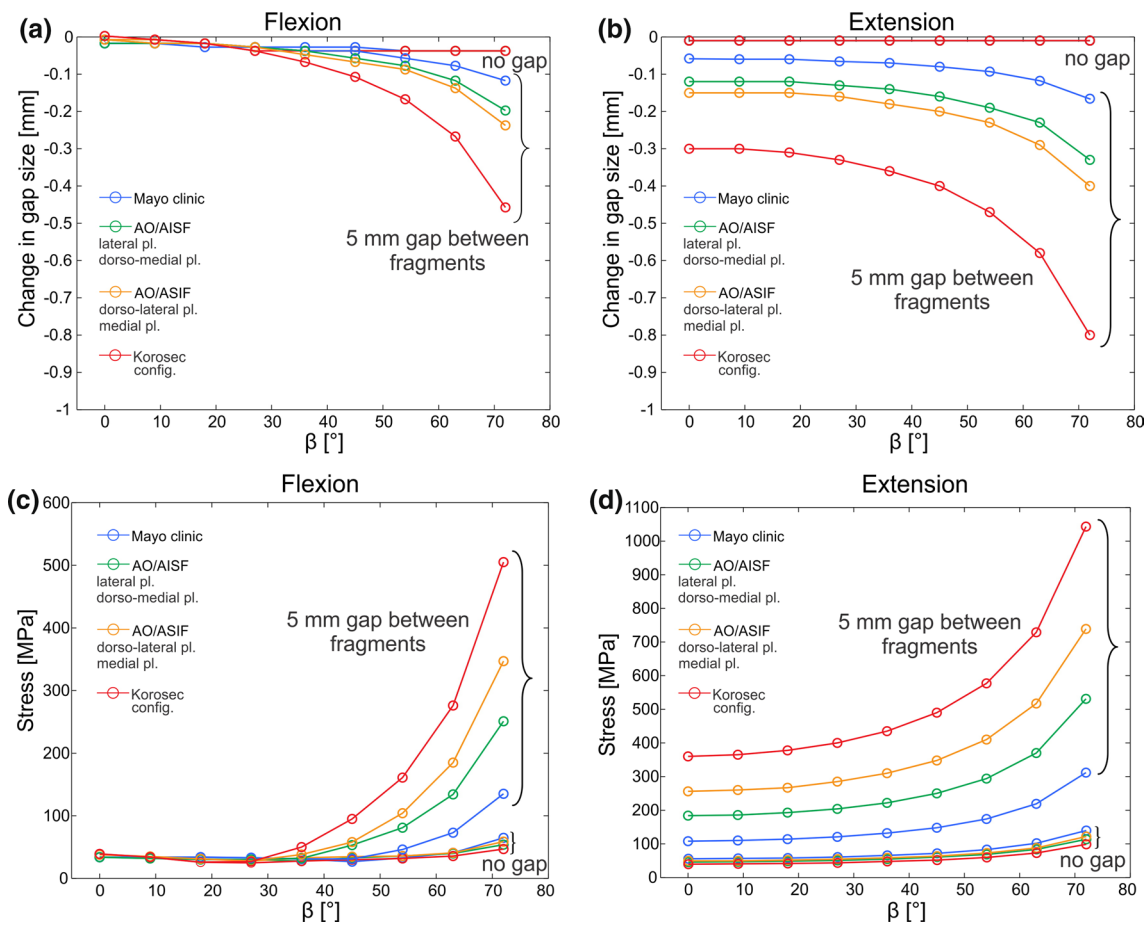
Fig. 5 Changes in gap size on the anterior side: **a** flexion, **b** extension. Maximal stresses in plates during: **c** flexion, **d** extension

16]. Note that plate configuration affects both the rigidity of the osteosynthesis construct and the invasiveness of the surgical procedure, which together influence the clinical outcome. A rigid osteosynthesis construct is important for stabilizing the bone fragments to allow early motion and enable patients to start with physiotherapy as soon as possible. Long durations of immobilization usually result in unsatisfactory elbow function and should be prevented. It should be also mentioned that too rigid construct can in certain cases also delay union or even result in nonunion [3]. In cases with no gap between fragments (or with minimal gap), the construct will enable bone to heal by primary healing (no significant callus formation). In cases where perfect or near perfect contact between fragments cannot be achieved, 180° system may create too stiff construct of fracture fixation that may lead to delayed union or nonunion. In fractures with a gap between fragments (missing fragments, significant comminution, etc.), it is necessary to create a construct or fixation of fragments, which will allow micro-movements in-between fragments and allow fracture healing by callus formation. Prevention of micro-movements (too stiff construct) may lead to nonunion of

fragments and consequent failure of fixation, requiring further operative intervention [3]. Moreover, access to the distal humerus demands a certain level of exposure as soft tissues are dissected. The more the plates are pushed toward the anterior (volar) part of the distal humerus (closer to 180° between plates, which comprises a more rigid osteosynthesis construct as quantified in our study) the more invasive the surgery that is required, causing higher operative trauma with early and late postoperative consequences such as scarring, limited range of movement and tardy ulnar nerve palsy. There is no common agreement between surgeons which plate configuration brings the best clinical outcome.

Different studies have experimentally compared plate configurations (Korner et al. [14], Penzkofer et al. [24], Schwartz et al. [25], Zalavras et al. [31]—results of these studies are described in the Introduction) aiming to find and justify the best method from a mechanical point of view. All these studies implemented gaps between bone fragments, to simulate no force transmission between fragments, i.e., to simulate multifragmentary fractures, where assembly of small bone parts is not practically feasible.

According to our experiences (clinical experiences of senior author M. K.), these cases represent only 1/3 of multi-fragmentary fractures of distal humerus. Approximately 2/3 of fracture cases can be reduced without a major defect in bone continuity, which means that part of the load can be transmitted over the contact between the bone fragments. For intraarticular fractures, we are looking toward inter-fragmentary compression to minimize callus formation and enable as normal as possible restoration of joint anatomy.

Our main goal was to investigate the rigidity of four osteosynthesis constructs using different plate configurations; firstly, with a gap between the bone fragments to verify experimental studies and secondly, with bone contact between the fragments to simulate the 2/3 s of real-life situations. A theoretical model was set up by implementing as real as possible load states, geometric models and material parameters. Three different extremity movements were examined: flexion, extension and the movement when the humerus is exposed to maximal torsion load. We compared all three systems with and without a gap in-between the proximal and distal bone fragments. We showed that gap change during the movement that induces torsional load is much smaller than during extension or flexion. During loading in flexion and extension, the gap between distal and proximal parts of the bone is decreasing due to the large axial compression, which dominates over shear and bending. Gap closing is the most prominent in the case of the Korosec configuration, less in both AO/ASIF configurations and least in the Mayo clinic plate configuration, which designates the rigidity of each system. This effect can be contributed to the bending moment, which is induced by the axial force, due to the particular position of the plates on the outer contour of the bone's cross-section. Namely, in the case of the Korosec plate configuration, lever distance between the axial load point, located in the centroid of the bone's cross-section, and the centroid of both plates, is the largest, followed by the AO/ASIF configuration. Particularly, in the Mayo clinic plate configuration, the lever distance is practically zero, meaning practically zero bending moment is induced by the axial force, and therefore, this system exhibits largest rigidity. Our results slightly differ from experimental findings of Korner et al. [14], Penzkofer et al. [24], Schwartz et al. [25], Zalavras et al. [31] (which also differ among themselves), but not in all loading/plate orientation cases. The differences we observe can be attributed to different loading conditions applied in each study. It is important to note that all of these experimental studies assumed simple loading conditions: pure axial, pure bending or pure torsion, whereas real loading conditions acting on the humerus are more complex—every muscle acts on the humerus at the point of attachment with a force, which depends on current upper extremity position. We tried to simulate real-life conditions within our theoretical model

as much as possible. For example, Korner et al. [14] measured no significant differences in rigidity between the AO/ASIF and Korosec (dorsal) plate configurations, when the construct was subjected to pure axial compression. In contrast, our theoretical study shows that axial compression contributes the most to the overall mechanical behavior of the system (this is the reason why the Mayo clinic system is the most, and the Korosec plate system is the least rigid system, see the comment above). We speculate that the reason is that in these experimental studies, applied forces were not large enough to observe characteristic differences (other than statistical) in rigidity of the plating systems. They applied the loads directly on the humerus, which means, e.g., that in the case of 300 N axial compression load applied directly to the axis of the humerus means 300 N of inner axial force. In contrast, we applied a load of 20 N in the center of the wrist and the complex forearm–humerus–muscle system transferred the load onto the humerus. We obtained larger values of inner axial force (as well as inner shear force and inner bending moment) for various upper extremity positions, as shown in Fig. 4.

On the other hand, in cases with no gap, the distal and proximal bone parts are in contact during loading, further displacements of each end are diminished, and the bone–bone fragments complex can carry a larger part of the forces, which significantly reduces the stress in the plates. But most importantly, there is no effect of axial force inducing additional bending moment, as in the case with a gap, which is reflected in the results showing similar mechanical responses in all plate configurations, as shown in Fig. 5. According to the best of the authors' knowledge, no studies exist in the available literature where a bone contact in-between the bone fragments is considered.

To reiterate, our results show that the most rigid configuration in a case with a gap between the bone fragments is the Mayo clinic plate configuration, followed by both AO/ASIF plate configurations, and the least rigid system is the Korosec plate configuration. The Korosec plate configuration is thus questionable for practical use because of its inferior rigidity. For this type of fracture, more invasive configurations (Mayo clinic and AO/ASIF configurations) are acceptable, which is already proven by many clinical implementations/realizations. Further studies should be done to predict which gap size change is still allowable, before Korosec plate configuration cannot be used. These studies should employ more realistic models, and importantly, more realistic in vitro measurements. On the other hand, we showed that when the humerus is reconstructed without a major defect in the bone continuity (approximately 2/3 s of real-life cases), contact between bone fragments can importantly contribute to overall osteosynthesis construct rigidity. In these cases, results in Fig. 5 show that differences in rigidity (and therefore changes in the gap

size) between different plate configurations become negligible. Therefore, when the contact between bone fragments exists, the best clinical outcome is expected for Korosec plate configuration because its mechanical performance is practically identical to other plate configurations, but its fixation requires significantly less exposure of soft tissues.

Within this model, we tried to simulate as real conditions as possible, but simple enough for the purposes of our study. Nevertheless, certain aspects of the model can be further improved, for example: modeling of contacts with friction between surfaces, especially contacts between bone fragments and contacts between screws and bone tissue; instead of tie constraints between screws and bone tissue, even more realistic conditions can be modeled; only compressive and shear stresses (no tensile) should be transferred between parts in contact; in practice, screws also induce some prestress, which influences the load carrying capacity of the screw–bone construct; additionally, a higher number and more complex geometry of bone fragments can be modeled; and a more accurate model of the mechanical properties of trabecular and cortical bone can be employed, including the effects of osteoporosis; given the presented theoretical modeling, one could also provide custom-made plates, optimized for each individual fracture case.

5 Conclusions

In our study, we address the question of which plate configuration is the most rigid, and how does the contact between the bone fragments affect the results. Based on theoretical calculations using engineering construction principles and finite element method, we present qualitative and quantitative estimations of the biomechanical response of four different configurations subjected to three different loading regimes for two different fracture cases, one with and one without a bone gap at the fracture site. In the case of a gap, which represents approximately 1/3 of real cases, our study shows that the Mayo clinic 180° plate configuration is the most rigid system during flexion and extension, followed by both AO/ASIF orthogonal plate configurations. The system with the lowest rigidity is the Korosec system with the plates on the dorsal side of the humerus. On the other hand, we find no significant differences in rigidity between the fixation configurations in the case of no gap in-between the bone fragments. We can therefore conclude that the contact between bone fragments may under certain conditions compensate for the lack of load carrying capacity of the implants. This finding may also help to answer an old question of how, in some cases, a construct involving highly osteoporotic bone fragments can withstand the loading during rehabilitation. We speculate that despite the fact that an implant cannot be

fixed very firmly (e.g., by screws) to such mechanically disadvantaged bone, the contact between the fragments may significantly lower the stress at the fixation sites (in the vicinity of the screws/screw holes).

From a clinical point of view, it is important to emphasize that dorsal plating involves significantly lower operating trauma due to a smaller exposure. Based on the results of this paper, it is therefore a good choice of treatment for distal humerus fractures with no expected gap in-between the bone fragments after fixation. Nevertheless, it is for clinicians to decide which treatment to choose according to the fracture configuration, bone quality and patient's expectations.

Conflict of interest   None.

References

1. Baumgartner D, Lorenzetti SR, Mathys R, Gasser B, Stüssi E (2009) Refixation stability in shoulder hemiarthroplasty in case of four-part proximal humeral fracture. Med Biol Eng Comput 47:515–522
2. Bolsterlee B, Veeger HEJ, Chadwick EK (2013) Clinical applications of musculoskeletal modelling for the shoulder and upper limb. Med Biol Eng Comp 51:953–963
3. Bottlang M, Doornink J, Lujan TJ, Fitzpatrick DC, Marsh JL, Augat P, von Rechenberg B, Lesser M, Madey SM (2010) Effects of construct stiffness on healing of fractures stabilized with locking plates. J Bone Joint Surg Am 92:12–22
4. Carpenter JE, Wening JD, Mell AG, Langenderfer JE, Kuhn JE, Hughes RE (2005) Changes in the long head of the biceps tendon in rotator cuff tear shoulders. Clin Biomech 20:162–165
5. Cheng HYK, Lin CL, Lin YH, Chen ACY (2007) Biomechanical evaluation of the modified double-plating fixation for the distal radius fracture. Clin Biomech 22:510–517
6. Dunham CE, Takaki SE, Johnson JA, Dunning CE (2005) Mechanical properties of cancellous bone of the distal humerus. Clin Biomech 20:834–838
7. Ethier CR, Simmons CA (2007) Introductory biomechanics: from cells to organisms. Cambridge University Press, Cambridge
8. Floyd RT, Thomson CW (1998) Manual of structural kinesiology. WBC/McFraw-Hill, New York
9. Gefen A (2002) Computational simulations of stress shielding and bone resorption around existing and computer-designed orthopaedic screws. Med Biol Eng Comput 40:311–322
10. Greco GD, de Las Casas EB, Cornacchia TPM, de Magalhaes CS, Moreira AN (2012) Standard disocclusion in complete dentures supported by implants without free distal ends: analysis by the finite elements method. J Appl Oral Sci 20:64–69
11. Hamill J, Knutzen KM (2009) Biomechanical basis of human movement. Wolters Kluwer Health/Lippincott Williams and Wilkins, Philadelphia
12. Huston RL (2009) Principles of biomechanics. Taylor & Francis, London
13. Korner J, Lill H, Müller LP, Rommens PM, Schneider E, Linke B (2003) The LCP-concept in the operative treatment of distal humerus fractures—biological, biomechanical and surgical aspects. Injury 34:S-B20–S-B30
14. Korner J, Diederichs G, Arzdorf M, Lill H, Josten C, Schneider E, Linke B (2004) A biomechanical evaluation of methods of distal humerus fracture fixation using locking compression

plates versus conventional reconstruction plates. J Orthop Trauma 18:286–293

15. Krkovic M, Bosnjak R (2008) Subperiosteal elevation of the ulnar nerve: anatomical considerations and preliminary results. Injury 39:761–767

16. Krkovic M, Kordas M, Tonin M, Bosnjak R (2006) Subperiosteal elevation of the ulnar nerve during internal fixation for fractures of the distal humerus assessed by intra-operative neurophysiological monitoring. J Bone Joint Surg Br 88(2):220–226

17. Lovard ST, Wagner JD, Baack B (2009) Biomechanical optimization of bone plates used in rigid fixation of mandibular fractures. J Oral Maxillofac Surg 67:973–985

18. MacLeod AR, Pankaj P, Simpson AHRW (2012) Does screw-bone interface modelling matter in finite element analysis? J Biomech 45:1712–1716

19. McGough RL, Debski RE, Taskiran E, Fu FH, Woo SLY (1996) Mechanical properties of the long head of the biceps tendon. Knee Surg Sports Traumatol Arthrosc 3:226–229

20. Netter FH (2005) Atlas of Human Anatomy. Data status, Ljubljana [publication in Slovene]

21. Nigg BM, Herzog W (1994) Biomechanics of the musculo-skeletal system. Wiley, Chichester

22. Nikooyan AA, Veeger HEJ, Chadwick EKJ, Praagmann M, van der Helm FCT (2011) Development of a comprehensive musculoskeletal model of the shoulder and elbow. Med Biol Eng Comput 49:1425–1435

23. O'Driscoll SW (2005) Optimizing stability in distal humeral fracture fixation. J Shoulder Elbow Surg 14:S186–S194

24. Penzkofer R, Hungerer S, Wipf F, von Oldenburg G, Augat P (2010) Anatomical plate configuration affects mechanical performance in distal humerus fractures. Clin Biomech 25:972–978

25. Schwarz A, Oka R, Odell T, Mahar A (2006) Biomechanical comparison of two different periarticular plating systems for stabilization of complex distal humerus fractures. Clin Biomech 21:950–955

26. Shin SJ, Sohn HS, Do NH (2010) A clinical comparison of two different double plating methods for intraarticular distal humerus fractures. J Shoulder Elbow Surg 19:2–9

27. Tai CL, Chen WP, Chen HH, Lin CY, Lee MS (2009) Biomechanical optimisation of different fixation modes for a proximal femoral L-osteotomy. BMC Musculoskelet Disord 10:112

28. Vandenbulcke F, Rahmoun J, Morvan H, Naceur H, Drazetic P, Fontaine C, Bry R (2012) On the mechanical characterization of human humerus using multi-scale continuum finite element model. In: 2012 IRCOBI conference, Dublin 2012, pp 598–610

29. Vandenbulcke F, Rahmoun J, Naceur H, Morvan H, Drazetic P, Fontaine C (2013) Multiscale modelling of the mechanical behaviour of human humerus under impact. Comput Methods Biomech Biomed Eng 16(Suppl 1):211–213

30. Wieding J, Souffrant R, Fritsche A, Mittelmeier W, Bader R (2012) Finite element analysis of osteosynthesis screw fixation in the bone stock: an appropriate method for automatic screw modelling. PLoS One 7(3):e33776

31. Zalavras CG, Vercillio MT, Jun BJ, Otarodifard K, Itamura JM, Lee TQ (2011) Biomechanical evaluation of parallel versus orthogonal plate fixation of intra-articular distal humerus fractures. J Shoulder Elbow Surg 20:12–20